Manganese L-Edge X-ray Absorption Spectroscopy of Manganese Catalase from *Lactobacillus plantarum* and Mixed Valence Manganese Complexes

M. M. Grush,[†] J. Chen,[†] T. L. Stemmler,[‡] S. J. George,[†] C. Y. Ralston,[†] R. T. Stibrany,[§] A. Gelasco,[‡] G. Christou,[||] S. M. Gorun,[§] J. E. Penner-Hahn,[‡] and S. P. Cramer*[,†,⊥]

Contribution from the Department of Applied Science, University of California, Davis, California 95616, Department of Chemistry, University of Michigan, Ann Arbor, Michigan 48109, Corporate Research Laboratories, Exxon Research and Engineering, Annadale, New Jersey 08801, Department of Chemistry, Indiana University, Bloomington, Indiana 47405, and Energy and Environment Division, Lawrence Berkeley Laboratory, Berkeley, California 94720

Received May 18, 1995[⊗]

Abstract: The first Mn L-edge absorption spectra of a Mn metalloprotein are presented in this paper. Both reduced and superoxidized Mn catalase have been examined by fluorescence-detected soft X-ray absorption spectroscopy, and their Mn L-edge spectra are dramatically different. The spectrum of reduced Mn(II)Mn(II) catalase has been interpreted by ligand field atomic multiplet calculations and by comparison to model compound spectra. The analysis finds a 10 *Dq* value of ∼1.1 eV, consistent with coordination by predominately nitrogen and oxygen donor ligands. For interpretation of mixed valence Mn spectra, an empirical simulation procedure based on the addition of homovalent model compound spectra has been developed and was tested on a variety of Mn complexes and superoxidized Mn catalase. This routine was also used to determine the oxidation state composition of the Mn in $[Ba_8Na_2ClMn_{16}(OH)_8(CO_3)_4L_8]\cdot 53H_2O$ (L = 1,3-diamino-2-hydroxypropane-*N*,*N*,*N*′,*N*′-tetraacetic acid).

Introduction

Manganese is a catalytic component of several enzymes, including catalase[1] and the oxygen-evolving complex of Photosystem II.[2] Catalases are responsible for the detoxification of hydrogen peroxide to molecular oxygen and water in aerobic cells.[1] Although most catalases are heme proteins, non-heme catalases have been purified from three species of bacteria, *Lactobacillus plantarum*,[3] *Thermoleophilum album*,[4] and *Thermus thermophilus*.[5] These systems are similar, and all contain a pair of manganese atoms at the active site. In *L. plantarum*, each dinuclear manganese site is contained in a 34 kDa subunit. These subunits are thought to be arranged in a homohexameric fashion.[6] It has been proposed that the native enzyme cycles between Mn(II)Mn(II) and Mn(III)Mn(III) oxidation states.[1] Optical spectroscopy results suggest that the two manganese atoms are linked by an oxo bridge in the Mn(III)Mn(III) form; this bridge may play a role in the mechanism.[1] Extended X-ray absorption fine structure (EXAFS) and electron spin echo envelope modulation studies on varius forms of catalase indicate the presence of at least one histidine imidazole ligand.[7,8] Both the reduced Mn(II)Mn(II) and a superoxidized Mn(III)Mn(IV) form are readily available for characterization and comparison with more complicated catalytic systems such as Photosystem II. Understanding the electronic structure of the Mn sites at different parts of the catalytic cycles, including the oxidation states, ligand fields, and magnetic couplings, is important for understanding the overall mechanism.

X-ray absorption spectroscopy has become a popular tool for investigating electronic and molecular structure in biological systems.[9] K-edge X-ray absorption near edge structure (XANES) and EXAFS have been reported for both Mn catalase[7] and Photosystem II.[2,10,11] In Photosystem II, however, the use of K-edge XANES to determine individual Mn oxidation states for the tetranuclear active site is complicated by the sensitivity of edge position to both electronic configuration and interatomic distances. Previous L-edge spectroscopy of Mn model compounds[12] found that the L-edge spectra were 3−4 times sharper than K-edges. Chemical shifts (∼2 eV per oxidation state), as

[†] University of California, Davis.
[‡] University of Michigan.
[§] Exxon Research and Engineering.
[||] Indiana University.
[⊥] Lawrence Berkeley Laboratory.
[⊗] Abstract published in *Advance ACS Abstracts,* December 1, 1995.

(1) Penner-Hahn, J. E. Structural Properties of the Mn site in the Mn Catalases. In *Mn Redox Enzymes*; Pecoraro, V. L., Ed.; VCH Publishers: New York, 1992.
(2) Debus, R. J. *Biochem. Biophys. Acta* **1992**, *1102*, 269−352 and references therein.
(3) Kono, Y.; Fridovich, I. *J. Biol. Chem.* **1983**, *258*, 6015−6019.
(4) Algood, G. S.; Perry, J. J. *J. Bacteriol.* **1986**, *168*, 563−567.
(5) Barynin, V. V.; Grebenko, A. I. *Dokl. Akad. Nauk. SSSR* **1986**, *286*, 461−464.
(6) Baldwin, E. Ph.D. Thesis, University of North Carolina, Chapel Hill, 1991.
(7) (a) Waldo, G. S.; Fronko, R. M.; Penner-Hahn, J. E. *Biochemistry* **1991**, *30*, 10486−10490. (b) Waldo, G. S.; Yu, S. Y.; Penner-Hahn, J. E. *J. Am. Chem. Soc.* **1992**, *114*, 5869−5870.
(8) (a) Dikanov, S. A.; Tsvetkov, Yu. D.; Khangulov, S. V.; Gol'dfeld, M. G. *Dokl. Akad. Nauk SSSR* **1988**, *302*, 1255−1257. (b) Stemmler, T. L.; Sturgeon, B. E.; Randall, D. W.; Britt, R. D.; Penner-Hahn, J. E. Manuscript in preparation.
(9) (a) Cramer, S. P. Biochemical Application of X-ray Absorption Spectroscopy. In *X-ray Absorption: Principles, Applications, Techniques of EXAFS, SEXAFS, and XANES*; Konigsberger, D. C., Prins, R., Eds.; John Wiley & Sons: New York, 1988. (b) Stohr, J. *NEXAFS Spectroscopy* Gomer, R., Ed.; Springer-Verlag: New York, 1992.
(10) Ono, T.; Noguchi, T.; Inoue, Y.; Kusinoki, M.; Matsushita, T.; Oyanagi, H. *Jpn. J. Appl. Phys., Part 1* **1993**, *32*, 530−532.
(11) (a) Yachandra, V. K.; Derose, V. J.; Latimer, M. J.; Mukerji, I.; Sauer, K.; Klein, M. P. *Science* **1993**, *260*, 675−679. (b) Riggs, P. J.; Mei, R.; Yocum, C. F.; Penner-Hahn, J. E. *J. Am. Chem. Soc.* **1992**, *114*, 10650−10651.

0002-7863/96/1518-0065$12.00/0

well as dramatically different line shapes, were seen for Mn(II), Mn(III), and Mn(IV).

This paper presents the L-edge spectra of Mn catalase—the first soft X-ray absorption spectra of a Mn metalloprotein. We also show that Mn L-edge spectra can be interpreted both theoretically and empirically. The theoretical simulations use ligand field atomic multiplet calculations with adjustable parameters for oxidation state, ligand field, and covalency. The empirical approach simulates the spectra of mixed valence clusters using representative Mn(II), Mn(III), and Mn(IV) model compound spectra. We have used these analysis procedures to interpret the L-edge spectra of Mn catalase in both the reduced and superoxidized forms.

Experimental Section

Sample Preparation. Mn catalase was purified from *L. Plantarum* as has been described by Kono et al.,[3] with the exception that chromatographic separation using fast flow Sepharose was performed instead of the initial batchwise DEAE extraction and a G-150 Sephadex column was added for final size exclusion. Samples were then concentrated to 35.9 mg/mL and assayed using a Clark-type oxygen electrode. The specific activity of these samples was typically 3600 AU/mg, where 1 activity unit (AU) corresponds to the decomposition of 1 μmol of H_2O_2/min, $[H_2O_2] = 20$ mM. The total Mn concentration was ~5 mM. Thin films of protein were dried on Si wafers. Activity measurements made on a rehydrated thin film of reduced Mn(II)Mn(II) catalase showed greater than 95% retention of the original activity. Analysis of a thin film of Mn(II)Mn(II) catalase which had been exposed to the beam for approximately 24 h, temperature cycled numerous times, exposed to ultrahigh vacuum, and rehydrated still showed 60−70% of the original specific activity.

$Mn_6O_2(O_2CPh)_{10}(py)_2(MeCN)_2$ and $Mn_4O_3Cl(O_2CMe)_3(dbm)_3$ were synthesized by S. Wang, $Mn_2O_2(O_2CMe)Cl_2(bpy)_2$ by M. W. Wemple, $Mn_3(O_2CPh)_2(biphen)_3(bpy)_3$ by A. R. Schake, and $NBu_4[Mn_4O_2(O_2CMe)_7(pic)_2]$ by E. Libby in the G. Christou lab.[13a−f] $[Mn_4(2\text{-}OHpicpn)_4](ClO4)_4$ was prepared by A. Gelasco in the V. L. Pecoraro lab.[14a,b] $[Ba_8Na_2ClMn_{16}(OH)_8(CO_3)_4L_8]\cdot 53H_2O$ (L = 1,3-diamino-2-hydroxypropane-*N*,*N*,*N*′,*N*′-tetraacetic acid), "Mn_{16}", was synthesized as described previously.[15] MnF_2, $MnSO_4$, and MnO_2 were used as obtained from Aldrich Chemical Co.

Data Collection. Protein spectra were recorded on undulator beamline X1B at the National Synchrotron Light Source,[16] with the undulator gap set at 41.5 mm, and on the soft X-ray station of wiggler beamline 10-1 at the Stanford Synchrotron Radiation Laboratory.[17] The beamline monochromator slits were set at 30 μm, corresponding to an ~0.29 eV resolution. The protein films were transferred to a cold finger inside the UHV chamber and placed at a glancing angle with respect to the incoming beam. A 2 or 4 μm Parylene ($-C_8H_8-$) filter was placed between the sample and the detector. This high-pass filter selectively removed the O fluorescence, at the expense of total flux and allowed us to probe the Mn fluorescence, as has been previously described.[18] Spectra were recorded by a Canberra Instruments 13-element Ge solid state detector,[18] with the single-channel analyzer windows set at the Mn Lα fluorescence energy. Samples were maintained at a temperature of ~30 K with a Janis cryostat. The reduced spectrum is a sum of a total of 10 scans, 4 s/point, while the superoxidized spectrum represents 12 scans, 6 s/point. Separate linear backgrounds have been subtracted from these spectra in the L_{III} and L_{II} regions. The L_{II} peak heights of these spectra have been arbitrarily normalized to unit intensity. The spectra of reduced and superoxidized catalase have been smoothed with windows of 0.2 and 0.5 eV, respectively. The 11 scans of photoreduced catalase were not smoothed.

Mn model compound spectra were taken on beamlines U4B[19] and X1B at the NSLS and on beamline 10-1 at SSRL with the beamline slits set at 15 μm or less, corresponding to beamline resolution of better than 0.16 eV. Finely powdered samples were affixed to Cu sample holders with the aid of Scotch double-sided sticky tape which was free of adventitious Mn. The sample holders were then mounted on the cold finger at an angle of 45° to the incident beam. Air-sensitive samples were prepared in either a N_2 glovebox or a glovebag filled with Ar and anaerobically loaded into the chamber via a load lock system. Spectra were recorded in electron yield mode using a Galileo 4716 channeltron electron multiplier mounted perpendicular to the sample. Linear backgrounds were subtracted from the 2−3 scans of each model compound in a fashion similar to that with the protein data. The spectra were again arbitrarily normalized to unity at the L_{II} peak.

All spectra were calibrated relative to the main peak of the L_{III} edge of MnF_2, which was assigned an energy of 640.0 eV.

Simulations. Atomic multiplet calculations were used to simulate Mn(II) spectra. These simulations assume transitions between a $2p^6$-$3d^5$ ground state and a $2p^53d^6$ excited state. Racah and RCN parameters were used as tabulated,[20] and the Slater integrals were set at 80% of the atomic values. The individual transitions were broadened with Lorentzians of 0.1 and 0.3 eV around the L_{III} and L_{II} regions, respectively, and convoluted with either a 0.15 or 0.30 eV Gaussian for model compounds and proteins, respectively. These broadening procedures compensated for both the inherent line width due to the lifetime of the final state and the beamline resolution. For the spectral analysis of manganese mixed valence complexes, an empirical simulation routine was used.

Results

Chemical Shifts. The shape and position of the Mn L-edges vary dramatically with oxidation state, as is shown in Figure 1. The L_{II} and L_{III} edges are due to electronic transitions to the 3d levels from the $2p_{1/2}$ and $2p_{3/2}$ levels, respectively. The additional complex features result from 2p−3d and 3d−3d Coulomb and exchange interactions, as well as crystal field effects.[21] High-spin Mn(II), as illustrated by $MnSO_4$ (Figure 1), exhibits a sharp peak near 640 eV with lesser peaks on both sides of the main L_{III} transition and a small L_{II} edge at higher energy. These features were reproduced by atomic multiplet calculations (Figure 1). In general, as the ligand field strength 10 *Dq* increases, the peaks in the wings split further away from the central line.[12]

(12) Cramer, S. P.; deGroot, F. M. F.; Ma, Y.; Chen, C. T.; Sette, F.; Kipke, C. A.; Eichhorn, D. M.; Chan, M. K.; Armstrong, W. H.; Libby, E.; Christou, G.; Brooker, S.; McKee, V.; Mullins, O. C.; Fuggle, J. C. *J. Am. Chem. Soc.* **1991**, *113*, 7937−7940.

(13) (a) Chemical abbreviations: Me = methyl, Ph = phenyl, py = pyridine, bpy = 2,2′-dipyridyl, biphen = 2,2′-biphenol, pic = picolinate, dbmh = dibenzoylmethane, NBu_4 = tetrabutylammonium. (b) Bashkin, J. S.; Schake, A. R.; Vincent, J. B.; Chang, H. R.; Li, Q.; Huffman, J. C.; Christou, G.; Hendrickson, D. N. *J. Chem. Soc., Chem. Commun.* **1988**, 700−702. (c) Hendrickson, D. N.; Christou, G.; Schmitt, E. A.; Libby, E.; Baskin, J. S.; Wang, S.; Tsai, H.-L.; Vincent, J. B.; Boyd, P. D. W.; Huffman, J. C.; Folting, K.; Li, Q.; Streib, W. E. *J. Am. Chem. Soc.* **1992**, *114*, 2455−2471. (d) Schake, A. R.; Vincent, J. B.; Li, Q.; Boyd, P. D. W.; Folting, K.; Huffman, J. C.; Hendrickson, D. N.; Christou, G. *Inorg. Chem.* **1989**, *28*, 1915−1923. (e) Christou, G. *Acc. Chem. Res.* **1989**, *22*, 328−335. (f) Libby, E.; McCusker, J. K.; Schmitt, E. A.; Folting, K.; Hendrickson, D. N.; Christou, G. *Inorg. Chem.* **1991**, *30*, 3486−3495.

(14) (a) Chemical abbreviations: picpn = picoliniminopropane. (b) Gelasco, A.; Askenas, A.; Pecoraro, V. L. *J. Am. Chem. Soc.* **1995**, submitted.

(15) (a) Gorun, S. M.; Stilbrany, R. T. Manuscript in preparation. A preliminary account of this work was presented at the ACS National Meeting, Atlanta, GA, 1991. (b) Gorun, S. M.; Stilbrany, R. T., U.S. Patent No. 5,041,575, 1991.

(16) Randall, K. J.; Eberhardt, W.; Feldhaus, J.; Erlebach, W.; Bradshaw, A. M.; Xu, Z.; Johnson, P. D.; Ma, Y. *Nucl. Instrum. Methods A* **1992**, *319*, 1−3:101−105.

(17) Karpenko, V.; Kinney, J. H.; Kulkarni, S.; Neufeld, K.; Poppe, C.; Tirsell, K. G.; Wong, J.; Cerino, J.; Troxel, T.; Yang, J.; Hoyer, E.; Green, M.; Humphries, D.; Marks, S.; Plate, D. *Rev. Sci. Instrum.* **1989**, *60*, 1451−1456.

(18) Cramer S. P.; Chen, J.; George, S. J.; van Elp, J.; Moore, J.; Tensch, O.; Colaresi, J.; Yocum, M.; Mullins, O. C.; Chen, C. T. *Nucl. Instrum. Methods A* **1992**, *319*, 1−3, 285−289.

(19) Chen, C. T.; Sette, F. *Rev. Sci. Instrum.* **1989**, *60*, 1616−1621.

(20) van der Laan, G.; Kirkman, I. W. *J. Phys.: Condens. Matter* **1992**, *4*, 4189−4204.

(21) deGroot, F. M. F.; Fuggle, J. C.; Thole, B. T.; Sawatzky, G. A. *Phys. Rev. B* **1990**, *42*, 5259−5468.

Table 1. Mixed-Valent Simulation Fitting Parameters

model compound	oxidation states	fit fraction	energy shift
$Mn_3(O_2CPh)_2(biphen)_3(bpy)_3$	$(II)(III)_2$	0.29 Mn(II)/total Mn	−0.09 eV (2+) −0.10 eV (3+)
$Mn_6O_2(O_2CPh)_{10}(py)_2(MeCN)_2$	$(II)_4(III)_2$	0.62 Mn(II)/total Mn	−0.06 eV (2+) +0.14 eV (3+)
$[Ba_8Na_2ClMn_{16}(OH)_8(CO_3)_4L_8]$	$(II)_{8.5}(III)_{7.5}$	0.49 Mn(II)/total Mn	+0.01 eV (2+) +0.02 eV (3+)
$Mn_2O_2(O_2CMe)Cl_2(bpy)_2$	(III)(IV)	0.39 Mn(III)/total Mn	−0.04 eV (3+) −0.08 eV (4+)
$Mn_4O_3Cl(OAc)_3(dbm)_3$	$(III)_3(IV)$	0.64 Mn(III)/total Mn	−0.01 eV (3+) +0.25 eV (4+)
Mn_2(III,IV) catalase	(III)(IV)	0.28 Mn(III)/total Mn	−0.62 eV (3+) −0.26 eV (4+)
Mn_2(III,IV) catalase (corrected for photoreduction)	(III)(IV)	0.36 Mn(III)/total Mn	+0.62 eV (3+) −0.17 eV (4+)

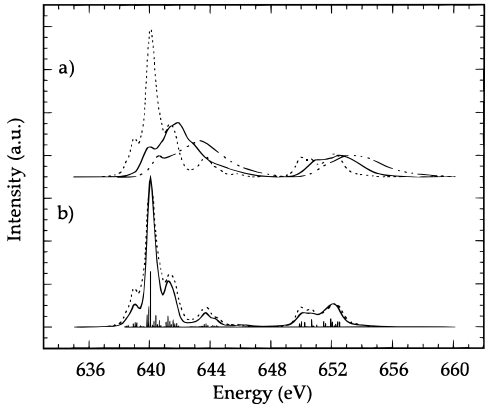

Figure 1. Oxidation state shifts of manganese L-edge spectra: (a) Mn(II)SO_4 (dotted line), $NBu_4[Mn(III)_4O_2(O_2CMe)_7(pic)_2]$ (solid line), and Mn(IV)O_2 (dotted and dashed line); (b) Mn(II)SO_4 (dotted line) and theoretical simulation (solid line).

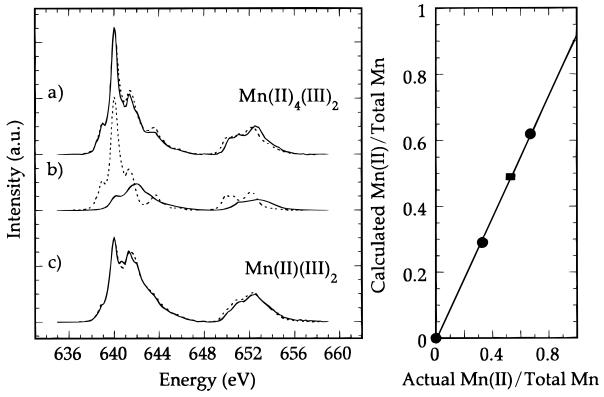

Figure 2. Simulations of $Mn(II)_xMn(III)_y$ model compounds. Left: (a) $Mn_6O_2(O_2Ph_{10})py_2(MeCN)_2$ (solid line) and simulation (dotted line), (b) Mn(II) component (dotted line) and Mn(III) component (solid line) of simulation for $Mn_6O_2(O_2Ph_{10})py_2(MeCN)_2$, and (c) $Mn_3(O_2CPh)_2(biphen)_3(bpy)_2$ (solid line) and simulation (dotted line). Right: fraction of Mn(II) to total Mn in best fit versus actual ratio of Mn(II) to total Mn in model compound. The horizontal bar corresponds to the ratio of Mn(II) to total Mn found for "Mn_{16}" using the empirical simulation routine.

Mn(III) and Mn(IV) have broad L-edge features which occur at higher energy than that of Mn(II), as is shown for $[Mn(III)_4O_2(O_2CMe)_7pic_2]$ and Mn(IV)O_2 (Figure 1). Charge transfer (covalency) and lower symmetry become more important for Mn(III) and Mn(IV), and therefore, simple octahedral ligand field multiplet calculations are less successful. More sophisticated procedures have been developed to account for charge transfer[22] but have yet to be satisfactorily applied to Mn(III) and Mn(IV). Instead, we have taken an empirical approach for interpretation of the mixed valence systems.

Mixed Valence Simulations. To fit a mixed valence spectrum, these simulations optimize the relative weights of homovalent experimental spectra, also allowing for small energy shifts. To calibrate the actual ratio of Mn oxidation states in the sample versus the fractions of normalized Mn single oxidation state spectra required for our experimental simulations, we first applied the procedure to a range of known mixed valence complexes. For simulations of $Mn(II)_x(III)_y$ spectra, we used a combination of Mn(II)SO_4 and $NBu_4[Mn(III)_4O_2(O_2CMe)_7(pic)_2]$ spectra as homovalent standards. The results from a series of fits are presented in Figure 2 and Table 1. As an example, the spectrum of the trinuclear mixed valence complex, $Mn_3(O_2CPh)(biphen)_3(bpy)_3$, is nicely simulated by a sum of $MnSO_4$ and $NBu_4[Mn(III)_4O_2(O_2CMe)_7pic_2]$ spectra. All of the main peaks are reproduced, as well as the ratio of L_{III} to L_{II} intensity. There is a slight discrepancy in the 641−642 eV range where the overall peak for the Mn(III) component is expected. In other model compound work, we have seen that the shape of the Mn(III) L_{III} peak is sensitive to the nature of the axial ligand in Jahn−Teller distorted complexes. A more elaborate simulation procedure would use a range of models with different ligand field parameters (10 *Dq*, *Ds*, etc.), but for the present application, the fit is more than adequate.

Although the component peak energies were allowed to vary in our simulation algorithm, for the $Mn(II)_x(III)_y$ simulations, they varied very little. This is consistent with trapped valence Mn species with little delocalization across metal centers, similar to results with most oxygen-bridged dinuclear iron complexes.[23] In contrast, in the fully delocalized $[Fe_2(Me_3tacn)_2(m\text{-}OH)_3][BPh_4]_2$ complex, the individual Fe(II) and Fe(III) peak positions move on the order of 0.6 eV closer together compared to isolated Fe(II) and Fe(III) spectra and coalesce into a single broad profile.[23]

The fractional ratios of monovalent Mn(II) to Mn(III) needed in the best fit do not correspond to the actual ratios, as arbitrarily normalizing the height of the L_{II} edge to unity does not take into account the decrease in branching ratio (L_{III} intensity/total line strength) with increase in oxidation state of Mn. We therefore calibrated the spectral ratio by finding the best scale factor using a linear regression. We also included the origin for our linear regression of the data as simulations on trivalent manganese did indeed yield a value of zero for the Mn(II) component. We were able to achieve a high level of correlation

(22) (a) DeGroot, F. M. F.; Fontaine, A.; Kao, C. C.; Krisch, M. *J. Phys.: Condens. Matter* **1994**, *6*, 6875−6884. (b) Kawai, J.; Takami, M.; Satoko, C. *Phys. Rev. Lett.* **1990**, *65*, 2193−2196.

(23) Peng, G.; van Elp, J.; Jang, H.; Que, L., Jr.; Armstrong, W. H.; Cramer, S. P. *J. Am. Chem. Soc.* **1995**, *117*, 2515−2519.

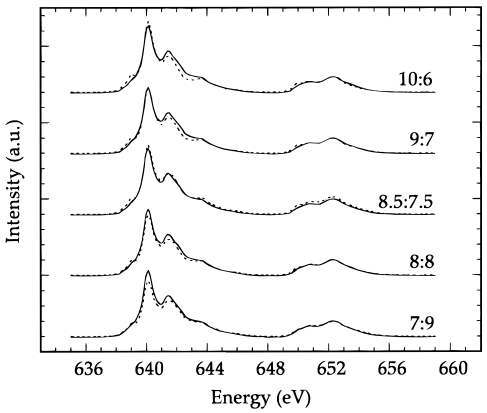

Figure 3. Simulations of $[Ba_8Na_2ClMn_{16}(OH)_8(CO_3)_4L_8]\cdot 53H_2O$ (L = 1,3-diamino-2-hydroxypropane-*N*,*N*,*N*′,*N*′-tetraacetic acid). Top to bottom: "Mn_{16}" (solid line) and simulation with a Mn(II)/Mn(III) ratio of 10:6 (dotted line); "Mn_{16}" (solid line) and simulation with a Mn(II)/Mn(III) ratio of 9:7 (dotted line); "Mn_{16}" (solid line) and best fit simulation with a Mn(II)/Mn(III) ratio of 8.5:7.5 (dotted line); "Mn_{16}" (solid line) and simulation with a Mn(II)/Mn(III) ratio of 8:8 (dotted line; and "Mn_{16}" (solid line) and simulation with a Mn(II)/Mn(III) ratio of 7:9 (dotted line).

($r^2 = 0.999$) in these fits which mimic the shape of the experimental spectra well. Taking into account the scatter in the data, we expect to be able to determine the Mn(II) fit fraction in an unknown $Mn(II)_x(III)_y$ compound to within ± 0.01 of the actual value.

We have used this algorithm to determine the oxidation state composition of the mixed valence "Mn_{16}" compound. This complex is the largest structurally characterized polynuclear Mn aggregate to date and consists of pentagonal bipyramidal Mn(II) sites and octahedral Mn(III) sites. The best simulation had a spectral ratio of 0.49 Mn(II)/total Mn which corresponds to a ratio of 8.5 ± 0.2 Mn(II) to 7.5 ± 0.2 Mn(III). The energy shifts were negligible, being +0.01 and +0.02 eV for the Mn(II) and Mn(III) components, respectively. Both single crystal X-ray diffraction measurements and elemental analysis of "Mn_{16}" support a ratio of approximately 9:7.[24] Mn coordination geometries in closely related Mn complexes, as determined via X-ray and neutron diffraction, also support these oxidation state assignments.[24,25] Figure 3 presents the best fit to the data and also compares simulations with Mn(II) to Mn(III) ratios of 10:6, 9:7, 8:8, and 7:9 to the data.

We have also applied this technique to mixed valence $Mn(III)_a(IV)_b$ spectra. The results of fitting with $NBu_4[Mn(III)_4O_2(O_2CMe)_7(pic)_2]$ and $Mn(IV)O_2$ are shown in Figure 4 and tabulated in Table 1. For example, the spectrum of the dinuclear mixed valence complex $Mn_2O_2(OAc)Cl_2(bpy)_2$ was simulated by a sum of $NBu_4[Mn(III)_4O_2(O_2CMe)_7(pic)_2]$ and $Mn(IV)O_2$ spectra. Both the general shape of the spectrum and the ratio of L_{III} to L_{II} intensity are reproduced in the simulations. However, there is some discrepancy on both sides of the L_{III} peak and also in the L_{II} region. These differences arise because the homovalent standards have broad features which cannot reproduce all of the mixed valence structure. There may also be some delocalization between the metal centers. However, since the energy shifts are less than 0.1 eV, these clusters are not highly delocalized. One exception is the 0.25 eV energy shift for the Mn(IV) component of the $Mn_4O_3Cl(O_2CMe)_3(dbm)_3$ simulation. As this shift is positive, it is more likely to be the effect of metal to ligand charge transfer than metal−metal delocalization. As before, the origin was induced in the linear regression ($r^2 = 0.980$). The scatter in the data corresponds to an uncertainty of ±0.02 in determining the Mn(III) fit fraction for an unknown $Mn(III)_a(IV)_b$ compound.

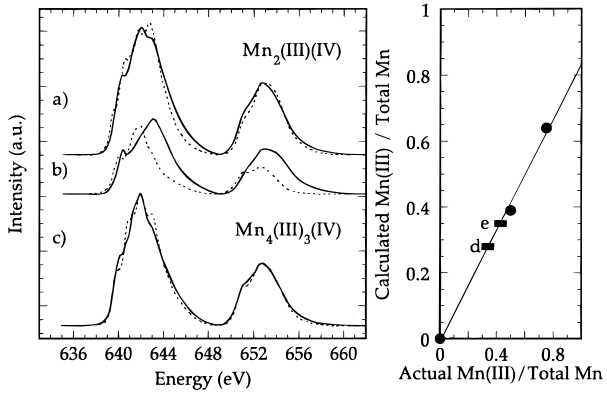

Figure 4. Simulations of $Mn(III)_aMn(IV)_b$ model compounds. Left: (a) $Mn_2O_2(OAc)Cl_2(bpy)_2$ (solid line) and simulation (dotted line), (b) Mn(III) component (dotted line) and Mn(IV) component (solid line) of simulation for $Mn_2O_2(OAc)Cl_2(bpy)_2$, and (c) $Mn_4O_3Cl(OAc)_3(dbm)_3$ (solid line) and simulation (dotted line). Right: fraction of Mn(III) to total Mn in best fit versus actual ratio of Mn(III) to total Mn in model compound. The horizontal bars correspond to the fraction of Mn(III) to total Mn found for (d) superoxidized Mn catalase and (e) superoxidized catalase, which has been corrected for photoreduction.

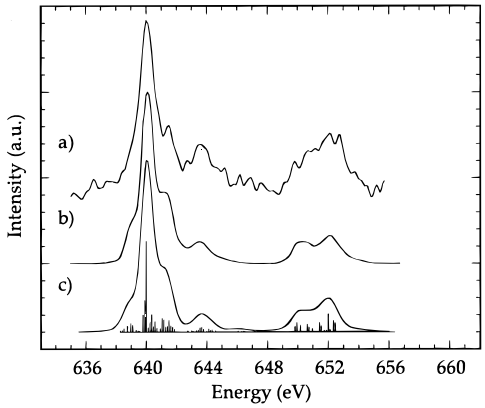

Figure 5. Mn(II)Mn(II) L-edge absorption spectra: (a) Mn(II)Mn(II) catalase, (b) $[Mn_4(2\text{-}OHpicpn)_4](ClO4)_4$, a Mn(II)Mn(II) dimer of dimers, and (c) atomic multiplet simulation of Mn(II)Mn(II) catalase, theoretical calculation (sticks), and smoothed theoretical spectrum (solid line).

Manganese(II,II) Catalase. The spectrum of Mn catalase in the reduced form is presented in Figure 5. The spectrum consists of a main L_{III} peak at 640 eV and a smaller L_{II} edge ~12 eV higher. Also shown for comparison are the spectrum from $[Mn_4(2\text{-}OHpicpn)_4](ClO4)_4$ and the results from atomic multiplet simulations on Mn(II)Mn(II) catalase. $[Mn_4(2\text{-}OHpicpn)_4](ClO4)_4$ is a so-called "dimer of dimers" model compound, consisting of divalent Mn with octahedral coordination. There are two resolved shoulders on the high-energy side of the L_{III} in this $[MnN_4O_2]$ compound, as well as an unresolved shoulder on the low-energy side. The L_{II} region is split into a doublet. These features are consistent with those from the Mn(II)Mn(II) catalase spectrum. Spectra of compounds with greater ionic character, such as $MnSO_4$, are very different from that of catalase, most noticeably in the presence

(24) Gorun, S. M.; Stibrany, R. T. U.S. Patent No. 5,099,045, 1991.
(25) Schulz, A. Unpublished neutron diffraction data; presented at the ACS National Meeting, San Diego, CA, 1994.
(26) (a) George, S. J.; Lowery, M. D.; Solomon, E. I.; Cramer, S. P. *J. Am. Chem. Soc.* **1993**, *115*, 2968−2969. (b) George, S. J.; van Elp, J.; Chen, J.; Ma, Y.; Chen, C. T.; Park, J.-B.; Adams, M. W. W.; Searle, B. G.; deGroot, F. M. F.; Fuggle, J. C.; Cramer, S. P. *J. Am. Chem. Soc.* **1992**, *114*, 4426−4427.

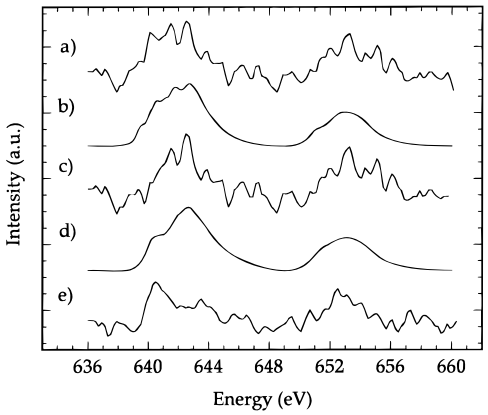

Figure 6. Mn(III)Mn(IV) L-edge absorption spectra: (a) Mn(III)Mn(IV) catalase, (b) $Mn_2O_2(OAc)Cl_2(bpy)_2$, a Mn(III)Mn(IV) dimer, (c) Mn(III)Mn(IV) catalase, which has been corrected to compensate for 8% photoreduction, (d) empirical mixed valence simulation of the corrected Mn(III)Mn(IV) catalase, and (e) Mn(III)Mn(IV) catalase which contains ~45% Mn(II) due to photoreduction.

of a low-energy shoulder that is resolved only in more ionic compounds (compare Figures 1 and 5).

A series of atomic multiplet calculations with varying octahedral ligand field values were performed. A ligand field value of 0.80 eV gave the best agreement to the experimental spectrum (Figure 5). As Mn L-edges have been shown to yield 10 *Dq* values ~25% smaller than those obtained from UV−vis spectroscopy,[12] our results correspond to an optical 10 *Dq* value of 1.1 eV. This number is consistent with predominately nitrogen and oxygen coordination to the Mn.[12]

The similarities between the protein data and that from $[Mn_4(2\text{-OHpicpn})_4](ClO4)_4$ suggest that this is a reasonable model for the Mn in reduced catalase. The spectra rule out extreme cases such as tetrahedral Mn or sulfur ligation. Modest covalent character with predominantly nitrogen and oxygen ligation is in agreement with current EXAFS results on reduced Mn catalase which suggest 2−4 imidazoles per Mn and possible bridging ligands of either (μ-carboxylato)$_n$ or (μ-OH)(μ-carboxylato)$_n$, where $n = 1-3$.[7]

Manganese(III,IV) Catalase. Figure 6 presents the spectrum of superoxidized Mn catalase. The L_{III} peak occurs ~2 eV higher in energy than in the reduced form, and the energy separation between the L_{III} and L_{II} is again ~12 eV. The Mn(II)Mn(II) protein spectrum is much sharper and has more intense L_{III} transitions than those associated with the broad spectrum obtained from the Mn(III)Mn(IV) form, as is expected. Also shown for comparison are $Mn_2O_2(OAc)Cl_2(bpy)_2$ and the results from the empirical mixed valence simulations. $Mn_2O_2(OAc)Cl_2(bpy)_2$ is a Mn(III)Mn(IV) dimer with octahedral coordination. This mixed valent dimer exhibits a broader spectrum than the divalent manganese, with the middle of the L_{III} region occurring at 642 eV and the L_{II} at 654 eV (Figure 6). The broad features of the Mn(III)Mn(IV) dimer are consistent with those from the superoxidized Mn catalase.

Using our mixed valence simulation routine, the best fit to the experimental spectrum of superoxidized Mn catalase corresponded to a Mn(III) to Mn(IV) ratio of 0.7 ± 0.1:1.3 ± 0.1 (Figure 6). The energy shift of the Mn(IV) component was −0.26 eV, while that of the Mn(III) component was larger, at −0.62 eV. A simple explanation for these relatively large negative energy shifts is that, even though care was taken to change the position of the protein frequently, some photoreduction by the X-ray beam occurred.

Photoreduction is an important concern for soft X-ray experiments and has been observed in other proteins, such as iron rubredoxin and blue copper proteins.[26] Figure 6 also shows a photoreduced Mn(III)Mn(IV) catalase sample which had been continuously in the beam for ~8 h. The main L_{III} feature at 640 eV in the bottom spectrum is due to Mn(II) from centers which have been photoreduced. From the mixed valence simulation routines, we estimate that on the order of 45% of the Mn has been photoreduced.

Upon subtraction of 8% Mn(II) from the superoxidized Mn catalase data, the correct ratio of 0.9 ± 0.1 Mn(III) to 1.1 ± 0.1 Mn(IV) is obtained from the simulation routines. Both of these spectra are presented in Figure 6. The relatively large energy shifts of the Mn(III) and Mn(IV) components toward each other (+0.62 and −0.17 eV) suggest that the Mn in superoxidized catalase is more delocalized than in $Mn_2O_2(OAc)Cl_2(bpy)_2$.

Conclusion and Prognosis

Mn L-edge spectroscopy is useful for characterization of the electronic structure of small molecules and metalloproteins. A theoretical approach is satisfactory for simulating pure Mn(II) samples, while for mixed valence complexes, an empirical approach is more practical.

The spectrum of reduced Mn(II)Mn(II) catalase was simulated with a ligand field of 0.80 eV (1.1 eV for an optical 10 *Dq* value). Experimental mixed valence simulations of the L-edge spectrum of "Mn_{16}" yielded a ratio of 8.5 Mn(II) to 7.5 Mn(III), which agrees with approximate measurements from other spectroscopies. When applied to the spectrum of superoxidized Mn(III)Mn(IV) catalase, the mixed valence simulation routine predicted a Mn(III) to Mn(IV) ratio of 0.7:1.3. After correction for ~8% photoreduction, the correct ratio of approximately 1 Mn(III) to 1 Mn(IV) was obtained. This interpretation of a mixed valence fluorescence spectrum using a simulation routine based on spectra taken by electron yield shows the promise of the fluorescence L-edge technique as applied to dilute protein samples, in spite of recent evidence[27] that there are minor differences between electron yield and fluorescence spectra. With more efficient detectors, photoreduction should be less of a problem and obtaining Mn L-edge spectra on more dilute systems such as Photosystem II should be feasible.

Acknowledgment. The authors would like to thank Y. Ma for help operating beamline X1B, H.-J. Lin for assistance with beamline U4B, J. Christiansen, G. Peng, and C. S. Bryant for help collecting data, J. Christiansen, M. W. Wemple, G. Peng, and M. J. Latimer for helpful scientific discussions, and B. Smith for help with word processing. This work was supported by the National Institutes of Health GM 44380 (S.P.C.), GM 45205 (J.E.P.-H.), and GM 39083 (G.C.) and the Department of Energy, Office of Health and Environmental Research. Both the National Synchrotron Light Source and the Stanford Synchrotron Radiation Laboratory are supported by the U.S. Department of Energy, Office of Basic Energy Sciences.

JA951614K

(27) deGroot, F.; Arrio, M. A.; Sainctavit, P.; Cartier, C.; Chen, C. T. *Solid State Commun.* **1994**, *92*, 991−995.